Highly-crystallized quaternary chalcopyrite nanocrystals *via* a high-temperature dissolution–reprecipitation route

J. Y. Chane-Ching,*[a] A. Gillorin,[a] O. Zaberca,[a] A. Balocchi[b] and X. Marie[b]

DOI: 10.1039/c1cc10749f

Quaternary chalcopyrite (Cu_2CoSnS_4, Cu_2ZnSnS_4) nanocrystals displaying high crystallization and controlled morphology were synthesized *via* a high-temperature growth regime achieved by dissolution–reprecipitation of tailored ultrafine precursors in the temperature range 400–500 °C.

Nanostructured cells are generally described as third-generation solar cells with the goal to significantly increase device efficiencies.[1] These cells include quantum-dot intermediate band solar cells,[1] hybrid cells[2] and involve the use of semiconducting inorganic nanocrystals. Recently, use of these semiconducting nanocrystals has been extended as inks[3] to replace more expensive non-vacuum techniques to the fabrication of thin film absorbers of second-generation cells. In these applications, surface and bulk properties of these nanocrystals are crucial for improving the efficiency of the nano-crystal-based devices. Regarding the bulk properties, electron–hole recombination which increases current losses, is very sensitive to the presence of defects. Thus, single-crystalline or highly crystallized nano-crystals are highly desirable for these photovoltaic applications. Indeed, a crucial point to increase efficiency of nanostructured solar cells is the ability to control the defect concentration of the semiconductor nanocrystals.[4] However, the limited available information relating to the defect concentration dependence of the photovoltaic properties is mainly due to the difficulty in preparing perfectly crystallized inorganic semiconducting nanocrystals. Therefore, it is important to develop new synthetic routes producing size and morphology controlled nanocrystals which exhibit high crystallization. Among candidate materials, ternary chalcopyrite nanocrystals[5] have attracted great attention because of their potential for use in solar cells. Most recently, quaternary chalcopyrite nanocrystals[6] displaying similar structure and optical properties to $CuInS_2$ are receiving considerable attention as promising candidates for low-cost absorber layers.[7] Cu_2ZnSnS_4 is one of the well-known quaternary chalcopyrites,[8] however, few reports describe the synthesis and properties of these nanocrystals.[6] The only reported synthetic routes[6,9] involve the arrested precipitation in coordinating solvent at temperatures of 200 °C. Nevertheless, UV-Vis absorption spectra recorded on the resulting nanocrystals did not exhibit any well-defined excitonic peak. The lack of a distinct excitonic peak could arise from various factors such as a large variation in size and composition of the quaternary chalcogenide nanocrystals, or from a too large defect concentration existing in these semiconductor nanocrystals, prepared at a relatively low temperature. Herein, we employ a high temperature (450 °C) dissolution–reprecipitation route performed in molten salts to sufficiently increase the crystallization of the nano-crystals such that a distinct excitonic peak can be observed in the UV-Vis absorption spectrum. Critically, the multiplication of nucleation centers resulting from the use of tailored ultrafine Cu_2MSnS_4 (M = Co, Zn) precursors affords to preserve the nanometric size of the crystals during the high-temperature crystallization stage. Moreover, a high-temperature growth regime was achieved for the size and morphology control of the Cu_2MSnS_4 nanocrystals *via* the use of a sulfide-source molten salt such as potassium thiocyanate, KSCN.

In our high-temperature crystallization process, high-temperature growth kinetics is achieved *via* the selection of a molten salt allowing a fine tuning of supersaturation conditions. Indeed, thermal decomposition of the melt KSCN occurs at temperatures >275 °C,[10] with cyanogen, sulfide and sulfur production. Thus, formation of quaternary chalcopyrite involves oxidation of the sulfur by the cyanide anion, with formation of the sulfide anion. A preliminary set of control experiments aimed at the formation of Cu_2MSnS_4 (M = Co, Zn) particles was performed using metal or metal oxides as metal precursors in KSCN and thiourea, $CS(NH_2)_2$. As expected,[11,12] all these experiments yielded only either microcrystalline or fully aggregated crystals. In general, nucleation and growth in dissolution–reprecipitation processes are significantly dependent on precursor dissolution kinetics, permitting size and morphology control of Cu_2MSnS_4 nanocrystals. Thus, in a first stage, ultrafine precursors displaying Cu_2MSnS_4 single phase and small primary crystallite size were synthesized from the polycondensation of charged complex species containing Cu^+, M^{n+}, Sn^{4+}, $CS(NH_2)_2$, S^{2-} and OH^- in various solvents such as ethylene glycol, ethanol and isopropanol. A variety of ultrafine precursors was synthesized consisting of 150–250 nm discrete, loose packed aggregates (Fig. 1) and displaying surface charge. Although all these

[a] *CIRIMAT, CNRS, INPT, Université de Toulouse, 118, Route de Narbonne, 31062 Toulouse Cedex 9*
[b] *LPCNO, INSA, CNRS, Université de Toulouse, 135, Avenue de Rangueil, 31077 Toulouse Cedex*

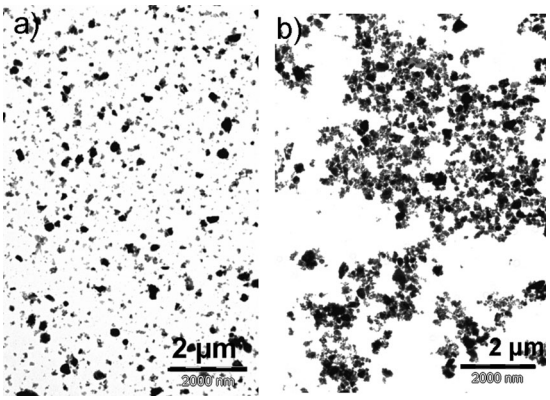

Fig. 1 TEM micrographs of (a) Cu_2CoSnS_4 precursors showing 150 nm discrete nanoparticles and (b) Cu_2ZnSnS_4 precursors with mean size of 250 nm.

precursors display a single phase as shown from XRD and Raman spectroscopy, slight differences in relative proportions in Raman peak surfaces located in the region 200–400 cm^{-1} and assigned to secondary and main Cu_2MSnS_4 vibrations[13] were observed. Further investigations are in progress to understand the origin of these short-range order differences. In a typical experiment, Cu_2CoSnS_4 ultrafine precursor was synthesized using the following molar ratios: 2.0 $CuCl_2 \cdot 2H_2O$: 1.0 $CoCl_2 \cdot 6H_2O$: 1.0 $SnCl_4 \cdot 5H_2O$: 10 $CS(NH_2)_2$: 1.0 TMAOH. The resulting mixture was transferred into a Teflon-line stainless steel autoclave for 16 h at 200 °C. The precipitated solid was washed and ball milled in EtOH using 0.3 mm ZrO_2 balls. After re-dispersion in EtOH, the ultrafine precursor was collected after size selection carried out by centrifugation at 3000 rpm. The particles were aggregates with a mean diameter of 150 nm (Fig. 1) and formed from primary crystallites of 6 nm average size, as calculated from Scherrer's equation using the full width at half maximum (FWHM) of the (112) Cu_2CoSnS_4 peak. In the second stage, the high-temperature growth stage was carried out in molten KSCN at 450 °C for 6 h. Because the molten salt acts as a sulfide source, a crucial parameter to control growth kinetics is the Cu_2CoSnS_4 nanocrystal volume fraction, $\Phi_{V_{nano}}$, $\Phi_{V_{nano}} = V_{nano}/(V_{nano} + V_{MS})$, where V_{nano} and V_{MS} denote, respectively, the volume occupied by the nanocrystals and the volume occupied by the molten salt. Indeed, $\Phi_{V_{nano}}$ dictates both the supersaturation level and the interparticle distance of the nanocrystals dispersed in the molten KSCN. High-temperature growth regimes were investigated for temperatures ranging from 300 to 550 °C and with various $\Phi_{V_{nano}}$ values, $0.045 < \Phi_{V_{nano}} < 0.17$. Formation of a Cu_2CoSnS_4 single phase was achieved up to 450 °C as demonstrated from XRD and Raman spectroscopy investigations. As expected, the high-temperature dissolution–reprecipitation process induces better crystallization as evidenced from the FWHM of the (112) Cu_2CoSnS_4 XRD peak. Moreover, a decrease of the FWHM (11.5 cm^{-1}) of the 327 cm^{-1} Raman main vibration (Fig. 2) indicates a significant improvement of the short-range order into the nanocrystals. Indeed, large variations in crystal size were observed depending on the chemical properties of the Cu_2CoSnS_4 precursors. Hence, nanocrystals were only produced with the use of precursors possessing Raman peak

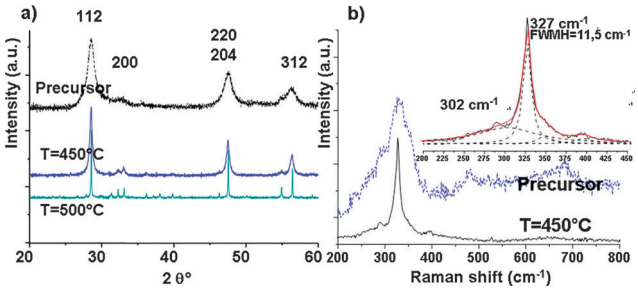

Fig. 2 (a) XRD pattern of highly crystallized Cu_2CoSnS_4 nanocrystals. (b) Raman spectrum of highly crystallized Cu_2CoSnS_4 nanocrystals. Inset: Deconvolution of the 200–400 nm region showing a main peak at 327 cm^{-1}. Corresponding XRD pattern and Raman spectrum of Cu_2CoSnS_4 precursors are indicated in dashed curves, highlighting the effect of the crystallization stage.

surface proportions similar to those determined from the bulk Cu_2CoSnS_4 spectrum.

Since the various precursors investigated exhibit similar size distributions, differences observed on the corresponding curves describing variation of the crystal size with dissolution–reprecipitation temperatures (Fig. 3) clearly indicate different dissolution kinetics for the Cu_2CoSnS_4 precursors. A power law increase of nanocrystal size with dissolution–reprecipitation temperature was observed for these highly homogeneous precursors. Our results indicate that the successful preparation of discrete nanocrystals rely on precursor properties such as an ultrafine size and a high short-range order as determined from Raman spectroscopy. A more uniform nanocrystal size distribution was achieved with careful control of $\Phi_{V_{nano}}$ (optimal value = 0.06), temperature and time. Typically, Cu_2CoSnS_4 solid precursor was mixed with KSCN (Aldrich, 99.99%) in a weight ratio of 1.00 : 5.00 and ground for 10 mn. The mixture was then placed within an alumina crucible which was subsequently heated to 450 °C for 6 h under N_2 atmosphere.

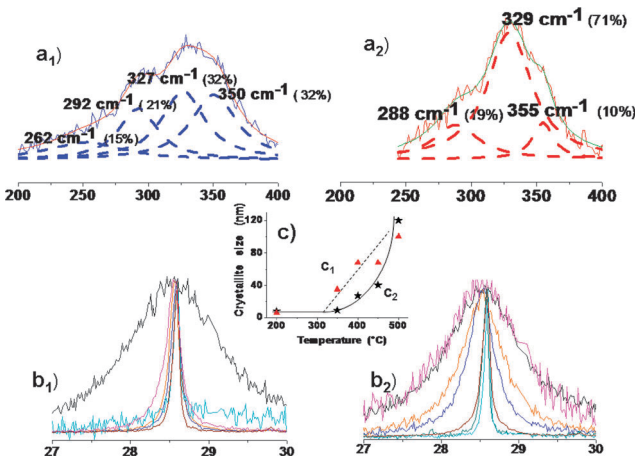

Fig. 3 (a) Cu_2CoSnS_4 precursor Raman spectra. (b) (112) Cu_2CoSnS_4 XRD peaks plotted as a function of dissolution–reprecipitation temperature. The Raman spectra and XRD peak evolutions correspond to samples displaying after deconvolution different (left figures a_1 and b_1) or similar (right figures a_2 and b_2) peak surface proportions compared with bulk Cu_2CoSnS_4. (c) Inset: XRD crystal size as a function of dissolution–reprecipitation temperature.

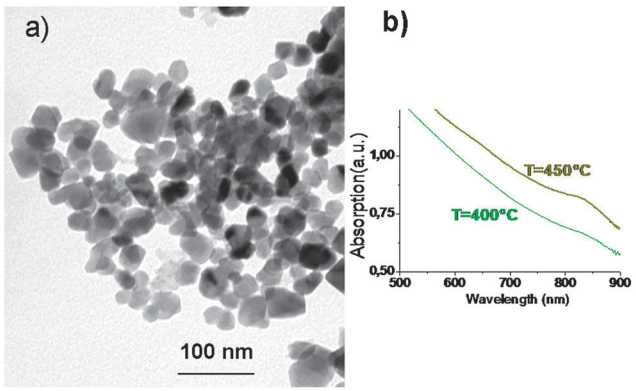

Fig. 4 Highly crystallized Cu_2CoSnS_4 nanocrystals. (a) TEM image showing discrete well faceted nanocrystals with a mean size of 30 nm. (b) UV-Vis absorption curve exhibiting a excitonic peak at 830 nm (1.5 eV).

After being cooled at room temperature, samples were subsequently washed with deionized water and ethanol. Transmission electron microscopy (TEM) images of the as-synthesized materials prepared using an ultrafine precursor show a uniform distribution of nanocrystals (Fig. 4). The particles were faceted and have a mean size as small as 30 ± 5 nm. From an XRD investigation and using the Scherrer formula, the size of the primary crystallites were determined to be 30 ± 2 nm, demonstrating that our nanocrystals are single crystals. Unlike previous quaternary chalcopyrite nanocrystals reported in the literature,[6] UV-Vis absorption spectra recorded on the Cu_2CoZnS_4 nanocrystals synthesized at high temperature exhibit a distinct excitonic peak observed at 830 nm (E_g = 1.5 eV). The observation of a well-defined absorption peak is the signature of both the high crystalline quality and the homogeneous composition of our nanocrystals.

The adaptability of the synthetic method was shown for the preparation of Cu_2ZnSnS_4 (CZTS) nanocrystals. A family of

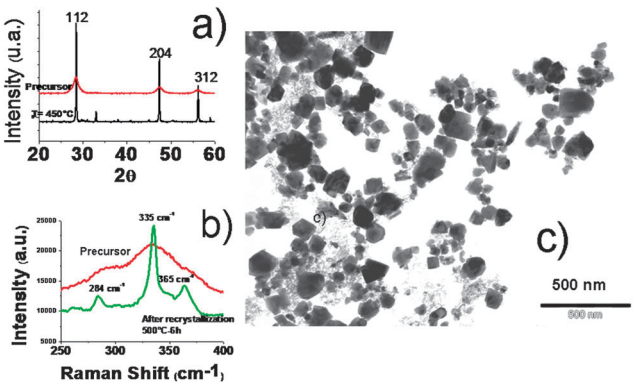

Fig. 5 Highly crystallized Cu_2ZnSnS_4 nanocrystals. (a) XRD pattern exhibiting a Cu_2ZnSnS_4 single phase. (b) Raman spectrum showing a major vibration at 335 cm^{-1}. Note the decrease of the FWHM of this 335 cm^{-1} peak compared with precursor (dashed curve) demonstrating an increase of the short range order of the nanocrystals. (c) TEM images showing discrete nanocrystals with well faceted shapes and a mean size around 150 mn.

CZTS precursors displaying controlled dissolution kinetic was prepared by varying the solvothermal reaction temperature (150–200 °C) and adjusting the [Cu^+] concentration. High-temperature growth regimes for dissolution–reprecipitation reactions were designed in the 400–500 °C temperature range and $\Phi_{V_{nano}}$ = 0.03–0.18, resulting in discrete CZTS nanocrystals with size ranging from 80 to 250 nm as shown by TEM (Fig. 5). The high crystallization of the nanocrystals is consistent with the features of the Raman spectrum displaying a low FMWH value (6 cm^{-1}) of the 335 cm^{-1} main peak assigned to Cu_2ZnSnS_4.[13] Further work involving precursors exhibiting smaller particle size, aimed towards the fabrication of Cu_2ZnSnS_4 single crystals, is in progress.

In conclusion, a high-temperature process involving the dissolution reprecipitation of Cu_2MSnS_4 (M = Co, Zn) ultrafine precursors was developed for the preparation of highly crystallized quaternary chalcogenide nanocrystals. Successful synthesis of 30 nm Cu_2MSnS_4 nanocrystals with controlled morphology was achieved through the fabrication of tailored precursors exhibiting ultrafine size and controlled dissolution kinetic.

We thank Alain Seraphine for very helpful discussions. This research was partly funded by Ecole des Beaux Arts et d'Architecture-Région la Reunion, France.

Notes and references

1 (*a*) A. Luque and A. Marti, *Phys. Rev. Lett.*, 1997, **78**, 5014; (*b*) A. J. Nozik, *Phys. E.*, 2002, **14**, 115; (*c*) R. P. Raffaelle, S. L. Castro, A. F. Hepp and S. G. Bailey, *Progr. Photovolt.: Res. Appl.*, 2002, **10**, 433.
2 W. U. Huynth, J. J. Dittmer and A. P. Alivisatos, *Science*, 2002, **295**, 2425.
3 (*a*) Q. Guo, S. J. Kim, M. Kar, W. N. Shafarman, R. W. Birkmira, E. A. Stach, R. Agrawal and H. W. Hillhouse, *Nano Lett.*, 2008, **8**, 2982; (*b*) M. G. Panthani, V. Akhavan, B. Goodfellow, J. P. Schmidtka, L. Dunn, A. Dodabalapur, P. F. Barbara and B. A. Korgel, *J. Am. Chem. Soc.*, 2008, **130**, 16770.
4 H. W. Schock and U. Rau, *Phys. B*, 2001, **308–310**, 1081.
5 (*a*) H. X. Schock, *MRS Bull.*, 1993, **28**(10), 42; (*b*) M. A. Contreras, B. Egaas, K. Ramanathan, J. Hiltner, A. Swartzlander, F. Hasoon and R. Noufi, *Progr. Photovolt.: Res. Appl.*, 1999, **7**, 311.
6 (*a*) O. Guo, H. W. Hillhouse and R. Agrawal, *J. Am. Chem. Soc.*, 2009, **131**, 11672; (*b*) C. Steinhagen, M. G. Panthani, V. Akhavan, B. Goodfellow, B. Koo and B. A. Korgel, *J. Am. Chem. Soc.*, 2009, **131**, 12554; (*c*) C. An, K. Tang, G. Shan, C. Wang, L. Huang and Y. Qian, *Mater. Res. Bull.*, 2003, **38**(5), 823.
7 (*a*) K. Ito and T. Nakazawa, *Jpn. J. Appl. Phys.*, 1988, **27**(Part 1, No. 11), 2094; (*b*) H. Katagiri, K. Jimbo, S. Yamada, Y. Kamimura, W. S. Maw, T. Fukano, T. Ito and T. Motohiro, *Appl. Phys. Express*, 2008, **1**, 041201; (*c*) T. K. Todorov, K. B. Reuter and D. B. Mitzi, *Adv. Mater.*, 2010, **22**, 1.
8 S. R. Hall, J. T. Szymanski and J. M. Stewart, *Can. Miner.*, 1978, **16**, 131.
9 A. Shavel, J. Arbiol and A. Cabot, *J. Am. Chem. Soc.*, 2010, **132**, 4514.
10 A. Eluard and B. Tremillon, *J. Electroanal. Chem.*, 1967, **13**, 208.
11 P. Boilac, V. Tanner and A. Garumann, *Cryst. Res. Technol.*, 1982, **17**(6), 717.
12 (*a*) J. Chen, X. Xing, A. Watson, W. Wang, R. Yu, J. Deng, L. Yan, S. Ce and Chen, *Chem. Mater.*, 2007, **19**(15), 3598; (*b*) H. Zhou, Y. Mao and S. S. Wong, *J. Mater. Chem.*, 2007, **17**, 1707.
13 M. Himmrich and H. Haeusler, *Spectrochim. Acta, Part A*, 1991, **47**, 933.